https://doi.org/10.20965/jrm.2021.p0274

Paper:

Feedback Control for a Drone with a Suspended Load via Hierarchical Linearization

Kazuma Sekiguchi, Wataru Eikyu, and Kenichiro Nonaka

Department of Mechanical Systems Engineering, Faculty of Engineering, Tokyo City University
1-28-1 Tamazutsumi, Setagaya-ku, Tokyo 158-8557, Japan
E-mail: ksekiguc@tcu.ac.jp

[Received September 23, 2020; accepted February 2, 2021]

As a possible extension of a drone application, transportation of a cable-suspended load is expected. The model of a drone with a suspended load is a nonlinear underactuated system that is known to be difficult to analyze and control. This paper applies the linearization method, known as hierarchical linearization, to the system. We observed that, via the hierarchical linearization scheme, the system can be linearized exactly and the controller can be designed simultaneously. There are two features of this approach. First, the controller exactly considers the system nonlinearity, and the feedback controller is based on the linear control theory. Second, it is possible to derive the analytical solution of the closed-loop system. We have demonstrated these features via numerical simulations.

Keywords: drone, cable-suspended load, hierarchical linearization, differential flatness

1. Introduction

With the advancement of microprocessors, the technology for drones, such as quadrotors, developed rapidly in the past decade. As a result, several applications and control methods have been proposed, as reviewed in [1, 2].

Transportation of external loads using drones is one of the most important applications [3, 4]. For example, transport of a cable-suspended load is an excellent way to retain the agility of a drone, and hence this type of drone has been actively studied [5–9].

Palunko et al. proposed the first practical controller for a drone with a cable-suspended load in [5]. Their study utilized adaptive control to endure a change in the center of gravity and proposed a dynamic programming-based trajectory generation to obtain a swing-free motion. A generation of a feasible reference trajectory is a fundamental problem in the application of a nonlinear underactuated system because the stabilizing controller can easily be extended to the reference trajectory tracking control. A geometric approach to design the feasible trajectory is introduced in [6], and a stabilizing controller for the trajectory is proposed in [6, 7]. Other approaches propose reinforcement learning [8] and nonlinear model predictive approach [9] as solutions to this control problem.

An approach based on a geometric property, known as differential flatness, was applied to generate a feasible reference trajectory in [6, 7]. A system is differentially flat if there exists a set of virtual outputs such that the system states and inputs can be expressed in terms of the flat output and a finite number of its time derivatives [10, 11]. This system property is advantageous not only in controller design [10] and state estimation [12], but also in the reference trajectory generation.

A drone with a suspended load is a nonlinear underactuated system, and it is known that the system is differentially flat. Therefore, the differential flatness-based approach is one of the most valuable ways to control the system. Differential-flatness means that a cable-suspended drone system is diffeomorphic to a linear system with a higher number of dimensions. This approach requires higher-order time derivatives of inputs to construct the diffeomorphism. In many cases, the differential flatness feature is utilized to design a feedforward control input or a feasible reference trajectory. In this case, we need an additional nonlinear controller to develop feedback control.

In this study, we adopted hierarchical linearization to establish decoupled linear subsystems. Hierarchical linearization was first introduced in [13]. It is a method that has an idea similar to that of linearization via a dynamic extension based on differential flatness. In particular, the dynamic extension gives a dynamics on the input to extend the relative degree. In contrast, our approach embeds the feedback controller into the input to extend the relative degree of the flat output [13, 14]. In other words there is no need to consider the input extension, and hence, the size of the linearized system is essentially equal to that of the original one. Therefore, the linear control theory was utilized to design the stabilizing controller.

Despite the abovementioned advantages of hierarchical linearization, the applicable systems' class is unclear and the design method of the hierarchical structure has not yet been established. In this study, we revealed that hierarchical linearization could be applied to a drone with a cable-suspended load by constructing a specific linearized system. Additionally, we analyzed the singularities that occur during the linearizing procedure.

© Fuji Technology Press Ltd. Creative Commons CC BY-ND: This is an Open Access article distributed under the terms of the Creative Commons Attribution-NoDerivatives 4.0 International License (http://creativecommons.org/licenses/by-nd/4.0/).

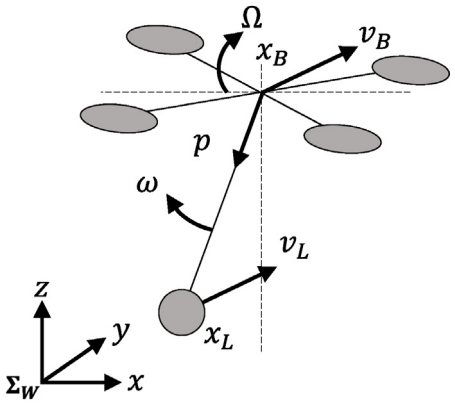

Fig. 1. A drone with a suspended load.

The reminder of this paper is organized as follows. Section 2 introduces the dynamics model of a drone with a suspended load. In Section 3, the linearized system and stabilizing controller are derived via the idea of hierarchical linearization. Section 4 illustrates the results of numerical simulations to verify the effectiveness of the proposed control structure and discusses the features of the proposed approach. Finally, Section 5 provides concluding remarks.

2. Suspended Load Model

A model of a drone with a load suspended by a stiff cable is shown in **Fig. 1**. We assumed that the cable weight is negligible. The load is modeled as a point mass and its attitude is not considered. With these assumptions, the dynamic model of a cable-suspended drone load was developed by Sreenath et al. [6, 7] as follows:

$$\dot{x}_L = v_L, \quad \ldots\ldots\ldots\ldots\ldots\ldots \quad (1)$$

$$(m_B + m_L)(\dot{v}_L + ge_3) = (p \cdot fRe_3 - m_B l(\dot{p}, \dot{p}))p, \quad (2)$$

$$\dot{p} = \omega \times p, \quad \ldots\ldots\ldots\ldots\ldots\ldots \quad (3)$$

$$m_B l \dot{\omega} = -p \times fRe_3, \quad \ldots\ldots\ldots\ldots\ldots\ldots \quad (4)$$

$$\dot{R} = R\hat{\Omega}, \quad \ldots\ldots\ldots\ldots\ldots\ldots \quad (5)$$

$$J_B\dot{\Omega} + \Omega \times J_B\Omega = M. \quad \ldots\ldots\ldots\ldots\ldots\ldots \quad (6)$$

The symbols used herein are explained in **Table 1**. $(\cdot,\cdot)$ indicates the inner product, and $\hat{\cdot}: \mathbb{R}^3 \to \mathfrak{so}(3)$ is defined such that $\hat{a}b = a \times b, \forall a, b \in \mathbb{R}^3$. Eqs. (1) and (2) represent the dynamics of the load, p illustrates the direction of the load with respect to the drone, and Eqs. (3)–(4) represents the load dynamics. Eqs. (5)–(6) are the drone attitude dynamics. The position of the drone is calculated using

$$x_B = x_L - lp, \quad \ldots\ldots\ldots\ldots\ldots\ldots \quad (7)$$

and the velocity v_B is calculated by substituting Eqs. (2) and (3) into a time derivative of Eq. (7).

The system has eight degrees of freedom with configuration space $SE(3) \times S^2$. In this study, the torsion of the cable is ignored; hence, the angular velocity ω around p is 0.

Table 1. Variables and their symbols.

Σ_W, Σ_B	Coordinate frame of world and body.
$x_L, v_L \in \mathbb{R}^3$	Position and velocity vectors of the center of load in Σ_W.
$x_B, v_B \in \mathbb{R}^3$	Position and velocity vectors of the center of mass of the drone in Σ_W.
$R \in SO(3)$	Rotation matrix that represents a posture of the drone in Σ_W.
$\Omega \in \mathbb{R}^3$	Angular velocity of the drone in Σ_B.
$\omega \in \mathbb{R}^3$	Angular velocity of the suspended load in Σ_W.
$p \in S^2 \subset \mathbb{R}^3$	Unit vector from the drone to the load in Σ_W.
$f \in \mathbb{R}$	Magnitude of the thrust force of the drone.
$M \in \mathbb{R}^3$	Moment vector for the drone in Σ_B.
$m_B \in \mathbb{R}$	Mass of the drone.
$m_L \in \mathbb{R}$	Mass of the suspended load.
$J_B \in \mathbb{R}$	Inertia matrix of the drone in Σ_B.
$l \in \mathbb{R}$	Cable length.
$e_1, e_2, e_3 \in \mathbb{R}^3$	Unit vectors along the x, y, z coordinate in Σ_W.
$q \in \mathbb{R}^4$	Unit quaternion corresponding to R.
$x \in \mathbb{R}^{19}$	State consisting of $[q^T, \Omega^T, x_L^T, v_L^T, p^T, \omega^T]^T$.
$u \in \mathbb{R}^4$	Input consisting of $[f, M^T]^T$.

3. Hierarchical Linearization

In this section, first, we present the algorithm of hierarchical linearization. Following this, we prove that the target system is linearizable via hierarchical linearization by deriving the linear subsystems specifically. Finally, the features of the proposed method are compared with those of the existing methods and the singularities that appeared in the procedures are analyzed.

3.1. Brief Idea of Linearization

Hierarchical linearization consists of two ideas called "directional decoupling" and "autonomization." Directional decoupling generates a subsystem that is isolated from the other subsystems. The rest of the subsystem may be effected from the subsystem. This is the meaning of "directional." In this procedure, the subsystem becomes the Brunovsky canonical form. "Autonomization" is defined as a procedure to make the isolated subsystem autonomous by designing and applying a feedback controller. For the rest of the subsystem, an autonomized subsystem serves as an exogenous signal generator. It is worth mentioning that the input designed in the autonomization procedure is no longer input for the remaining subsystem. Therefore, the geometric properties including the linearizability of the rest of the subsystem change via autonomization. Hierarchical linearization is an exact linearization method that repeats directional decoupling and autonomization. It is summarized as follows.

Algorithm: Hierarchical linearization [13, 14]

1. Directional decoupling: choose a function, and apply a partial feedback linearization to the function.

2. Autonomization: design and apply a controller to the subsystem linearized in Step 1.

3. If there is no input or no remaining freedom, then exit, else go back to Step 1.

This recursive loop is repeated at most the number of inputs. Therefore, this algorithm completes within a finite number of steps. Note that the choice of a function at the directional decoupling step, called virtual output, is an open problem. As discussed in [13, 14], although the hierarchical linearization method expands the class of linearizable nonlinear systems, it depends on the choice of virtual outputs.

3.2. Exact Linearization of a Drone with a Suspended Load

Fist, we transform the system into a state-space model as follows:

$$\dot{x} = f_0(x) + g_{01}(x)u_1 + g_{02}(x)u_2 + g_{03}(x)u_3 + g_{04}(x)u_4,$$

where x is the state vector consisting of the unit quaternion of attitude $q = [q_0, q_1, q_2, q_3]^T$, Ω and ω indicate the angular velocities of drone and load, respectively, p is the unit vector of load direction, $x_L = [x_{Lx}, x_{Ly}, x_{Lz}]^T$ and $v_L = [v_{Lx}, v_{Ly}, v_{Lz}]^T$ are the position and the translational velocity of the load. The time derivative of q is calculated as

$$\dot{q} = \frac{1}{2}\begin{bmatrix} -q_1 & q_0 & q_3 & -q_2 \\ -q_2 & -q_3 & q_0 & q_1 \\ -q_3 & q_2 & -q_1 & q_0 \end{bmatrix}^T \Omega.$$

The number of states is 19, and there are two norm constraints: $\|q\| = 1$ and $\|p\| = 1$. Because the cable rotation around p is ignored, the number of dimensions to be controlled is 16.

As revealed by Ishikawa et al. [15], the number of inputs must be greater than or equal to that of the dimensions of equilibria set for asymptotic stability with a time-invariant continuous state feedback controller. The equilibria set of the quadcopter system is given by

$$\left\{ x \;\middle|\; \begin{array}{c} v_L = 0, \Omega = 0, \omega = 0, \\ \|q\| = 1, q_1 = q_2 = 0, p = [0,0,-1]^T \end{array} \right\}.$$

The degree of freedom of the equilibria set is four, which corresponds to x_{Lx}, x_{Ly}, x_{Lz} and the rotation around the x_{Bz}-axis. This is equal to the number of inputs. Hence, we naturally chose x_{Lx}, x_{Ly}, x_{Lz} and the rotation angle around the x_{Bz}-axis as a controlled output. Indeed, these parameters are known as flat outputs for cable suspended drone systems. Therefore, we also adopted these variables as virtual outputs.

3.2.1. First Layer

As a virtual output for the first layer, we choose

$$h_1 = x_{Lz} - z_d(t),$$

where $z_d(t)$ denotes a time function of the desired load altitude. The time derivative of h_1 is calculated as follows:

$$\begin{aligned} \dot{h}_1 &= v_{Lz} - \dot{z}_d(t) \\ \ddot{h}_1 &= \bar{\mathscr{L}}_{f_0}\dot{h}_1 \\ &\quad + \begin{bmatrix} \mathscr{L}_{g_{01}}\dot{h}_1 & \mathscr{L}_{g_{02}}\dot{h}_1 & \mathscr{L}_{g_{03}}\dot{h}_1 & \mathscr{L}_{g_{04}}\dot{h}_1 \end{bmatrix} \begin{bmatrix} u_1 \\ u_2 \\ u_3 \\ u_4 \end{bmatrix} \end{aligned}$$

where $\mathscr{L}_a b$ is a Lie derivative of b along with a vector field a calculated using $\frac{\partial b}{\partial x}a$, and $\bar{\mathscr{L}}_a b := \mathscr{L}_a b + \partial b/\partial t$. In this layer, we are only concerned with z_L dynamics, and hence there appears only the thrust force term in its second time derivative; therefore $\mathscr{L}_{g_{02}}\dot{h}_1 = \mathscr{L}_{g_{03}}\dot{h}_1 = \mathscr{L}_{g_{04}}\dot{h}_1 = 0$. The dynamics with respect to h_1 is transformed into a Brunovsky canonical form with a two-dimensional state as follows:

$$\begin{aligned} \dot{\xi}_1 :&= \frac{\mathrm{d}}{\mathrm{d}t}\begin{bmatrix} h_1 \\ \dot{h}_1 \end{bmatrix} = \begin{bmatrix} 0 & 1 \\ 0 & 0 \end{bmatrix}\xi_1 + \begin{bmatrix} 0 \\ 1 \end{bmatrix} v_1, \\ &=: A_1\xi_1 + B_1 v_1, \quad \ldots\ldots\ldots\ldots \quad (8) \end{aligned}$$

where v_1 is a virtual input given by canceling the nonlinearity in $\ddot{h}_1$ as follows.

$$u_1 = \frac{v_1 + \ddot{z}_d(t) - \bar{\mathscr{L}}_{f_0}\dot{h}_1}{\mathscr{L}_{g_{01}}\dot{h}_1}. \quad \ldots\ldots\ldots\ldots \quad (9)$$

This input transformation has a singularity at $\beta_1 := \mathscr{L}_{g_{01}}\dot{h}_1 = 0$ and is detailed further in Section 3.3.

So far, the dynamics of ξ_1 is directionally decoupled from the other dynamics. This means that the other dynamics do not affect ξ_1 dynamics; instead they are affected by ξ_1 and v_1. Based on the linear control theory, we can easily establish a stabilizing controller as follows:

$$v_1 = F_1\xi_1, \quad \ldots\ldots\ldots\ldots\ldots\ldots \quad (10)$$

where F_1 is a feedback gain applied to ensure that the closed-loop system is asymptotically stable. By substituting the designed virtual input into Eq. (8), the subsystem of ξ_1 becomes autonomous. The autonomization of the first layer is thus completed.

Note that, in the ordinary exact linearization method, the design of a feedback controller is executed after the linearization is completed. On the other hand, in our linearization process, the design of feedback controller precedes the remaining linearization.

Finally, this entire system can be represented as follows:

$$\begin{aligned} \dot{x} &= f_1(x) + g_{12}(x)u_2 + g_{13}(x)u_3 + g_{14}(x)u_4, \quad (11) \\ f_1(x) &= f_0(x) + g_{01}(x)\frac{v_1 + \ddot{z}_d(t) - \bar{\mathscr{L}}_{f_0}\dot{h}_1}{\mathscr{L}_{g_{01}}\dot{h}_1}, \\ g_{1i}(x) &= g_{0i}(x) \qquad (i = 2,3,4). \end{aligned}$$

3.2.2. Second Layer

Based on the discussion of the equilibria set, we choose the following functions as virtual outputs for the second

layer:

$$
\begin{aligned}
h_2 &= x_{Lx} - x_d(t),\\
h_3 &= x_{Ly} - y_d(t),\\
h_4 &= \psi - \psi_d(t),
\end{aligned}
$$

where $x_d(t)$ and $y_d(t)$ are the horizontal references of the load position. The first term of h_4 denotes the yaw angle ψ and $\psi_d(t)$ is its reference.

We calculated the time derivatives of virtual outputs until the second layer inputs u_2, u_3, u_4 appeared as follows:

$$
\begin{aligned}
h_2^{(6)} &= \bar{\mathscr{L}}_{f_1}^{(6)} h_2 + \left(\mathscr{L}_{g_{12}} \bar{\mathscr{L}}_{f_1}^{(5)} h_2\right) u_2\\
&\quad + \left(\mathscr{L}_{g_{13}} \bar{\mathscr{L}}_{f_1}^{(5)} h_2\right) u_3 + \left(\mathscr{L}_{g_{14}} \bar{\mathscr{L}}_{f_1}^{(5)} h_2\right) u_4,\\
h_3^{(6)} &= \bar{\mathscr{L}}_{f_1}^{(6)} h_3 + \left(\mathscr{L}_{g_{12}} \bar{\mathscr{L}}_{f_1}^{(5)} h_3\right) u_2\\
&\quad + \left(\mathscr{L}_{g_{13}} \bar{\mathscr{L}}_{f_1}^{(5)} h_3\right) u_3 + \left(\mathscr{L}_{g_{14}} \bar{\mathscr{L}}_{f_1}^{(5)} h_3\right) u_4,\\
\ddot{h}_4 &= \bar{\mathscr{L}}_{f_1}^{(2)} h_4 + \left(\mathscr{L}_{g_{12}} \bar{\mathscr{L}}_{f_1} h_4\right) u_2\\
&\quad + \left(\mathscr{L}_{g_{13}} \bar{\mathscr{L}}_{f_1} h_4\right) u_3 + \left(\mathscr{L}_{g_{14}} \bar{\mathscr{L}}_{f_1} h_4\right) u_4,
\end{aligned}
$$

where $\bar{\mathscr{L}}_a^{(i)} b$ is a recursive calculation of Lie derivative defined as $\bar{\mathscr{L}}_a(\bar{\mathscr{L}}_a^{(i-1)} b)$ and $\bar{\mathscr{L}}_a^{(1)} b := \bar{\mathscr{L}}_a b$.

Using this calculation, we confirmed the relative degrees of the virtual outputs with respect to Eq. (11) to be 6, 6, and 2 respectively. This means that there exists static feedback transformation that realizes 14 dimensional Brunovsky canonical form with the linearizing indices 6, 6, and 2. Furthermore, the decoupling matrix is

$$
\beta_2 = \begin{bmatrix}
\mathscr{L}_{g_{12}} \bar{\mathscr{L}}_{f_1}^{(5)} h_2 & \mathscr{L}_{g_{13}} \bar{\mathscr{L}}_{f_1}^{(5)} h_2 & \mathscr{L}_{g_{14}} \bar{\mathscr{L}}_{f_1}^{(5)} h_2\\
\mathscr{L}_{g_{12}} \bar{\mathscr{L}}_{f_1}^{(5)} h_3 & \mathscr{L}_{g_{13}} \bar{\mathscr{L}}_{f_1}^{(5)} h_3 & \mathscr{L}_{g_{14}} \bar{\mathscr{L}}_{f_1}^{(5)} h_3\\
\mathscr{L}_{g_{12}} \bar{\mathscr{L}}_{f_1} h_4 & \mathscr{L}_{g_{13}} \bar{\mathscr{L}}_{f_1} h_4 & \mathscr{L}_{g_{14}} \bar{\mathscr{L}}_{f_1} h_4
\end{bmatrix} \quad \ldots\ldots\ldots\ldots\ldots\ldots\ldots\ldots\ldots\ldots (12)
$$

As defined in Eq. (11), f_1 includes $v_1(t)$, and therefore β_2 consists of v_1 and its time derivatives $\dot{v}_1, \ldots, v_1^{(6)}$. Generally, high-order time derivatives are difficult to calculate; however, in this method, v_1 has been designed at an autonomization step. Therefore, the i-th time derivative of v_1 is calculated as

$$
v_1^{(i)} = F_1 \xi_1^{(i)} = F_1 (A_1 + B_1 F_1)^{(i)} \xi_1, \quad \ldots\ldots (13)
$$

where A_1 and B_1 are system matrices defined in Eq. (8). If we apply the dynamic extension to the system, then the time derivatives of the actual inputs are required to construct the linearizing transformation. Compared to this, the proposed approach realizes a static feedback controller, which only requires state information.

Applying the following input transformation, we get:

$$
\begin{bmatrix} u_2\\ u_3\\ u_4 \end{bmatrix} = \beta_2^{-1} \left(- \begin{bmatrix} \bar{\mathscr{L}}_{f_1}^{(6)} h_2\\ \bar{\mathscr{L}}_{f_1}^{(6)} h_3\\ \bar{\mathscr{L}}_{f_1}^{(2)} h_4 \end{bmatrix} + \begin{bmatrix} v_2\\ v_3\\ v_4 \end{bmatrix} \right). \quad (14)
$$

Subsequently, we obtain the linear subsystems as follows:

$$
\begin{aligned}
h_2^{(6)} &= v_2, \quad \ldots\ldots\ldots\ldots\ldots\ldots (15)\\
h_3^{(6)} &= v_3, \quad \ldots\ldots\ldots\ldots\ldots\ldots (16)\\
h_4^{(2)} &= v_4. \quad \ldots\ldots\ldots\ldots\ldots\ldots (17)
\end{aligned}
$$

The number of states is 19, and there are norm constraints for the unit quaternion q, the direction of the load p, and the angular velocity ω. Hence, the number of states to be controlled is 16. Therefore, we achieved an exact linearization via a static feedback transformation.

3.3. Discussions

In this section, we discuss the singularity of the proposed method and compare it to other methods.

First, let us discuss the comparison with the dynamic extension-based controller. As mentioned in the previous section, the essential degree of dynamics is 16. The relative degree of the flat outputs $(x_{Lx}, x_{Ly}, x_{Lz}, \psi)$ is $(2,2,2,2)$, respectively; therefore, the system transforms into four linear subsystems with two dimensions following the standard static feedback linearization method. In comparison, the dynamic feedback linearization extends the linearizable dimension by considering the fourth time derivative of $u_1 = f$. Owing to this dynamics extension, the essential freedom of dynamics becomes 20, and the relative degree of the flat outputs becomes $(6,6,6,2)$. Hence, the extended system is diffeomorphic to a linear system.

Both the dynamic extension and the proposed approaches appear as time derivatives of input; however, there is one critical difference between them. The dynamic extension approach requires the values of the high-order differentials of u_1 to calculate the diffeomorphism. In contrast, in the proposed method, because the time derivative of v_1 is represented as Eq. (13), time derivative itself becomes unnecessary while calculating the actual input. Therefore, our approach can avoid a redundant time delay in the dynamic extension approach by adding dynamics into the input.

Second, let us compare the existing controller provided by Sreenath et al. [6, 7]. In their studies, the differential flatness is utilized to design the admissible reference trajectory, and a stabilizing controller for the trajectory has been proposed. In their method, a detailed additional analysis needs to be conducted to guarantee exponential stability. In our approach, the exponential stability is trivially guaranteed by the linear control theory, except in the case of the singularity explained in the remaining of the section. Moreover, we can represent the solution of the closed-loop dynamics analytically because the system is described with a static nonlinear transformation and a linear dynamical system.

Finally, we discuss the singularity that appears in the input transformation. From a physical viewpoint, the first layer consists of the dynamics of x_{Lz} with thrust input. In Eq. (9), the input transformation is singular at $\beta_1 := \mathscr{L}_{g_{01}} \dot{h}_1 = 0$, and it is satisfied when $p_3 = 0$ or $(p, Re_3) = 0$.

The first condition implies that the altitude of the load is equal to that of the drone. The second condition is the case where the load is on the rotor plane, and such a situation should be avoided to prevent the rotor from involving the cable.

The singularity in the second layer is formed as $\det(\beta_2) = 0$. The numerator of $\det(\beta_2)$ is represented as

$$R(3,3)N_1^2 N_2^2,$$

where

$$N_1 = v_1 + g + \ddot{z}_d,$$
$$N_2 = (m_L + m_B)N_1 + l m_B(\omega,\omega)p(3).$$

$R(3,3) = 0$ means the drone rotated by $\pi/2$ rad, and the direction of the thrust force is in the x-y plane in Σ_W. In this case, x_{B_z} cannot be controlled by the thrust, and it is reported in [14] that the same singularity appears in the drone controller realized via hierarchical linearization. The singularity $N_1 = 0$ implies that the acceleration of the load is $-g$. It is a free-fall condition of the load, which should be avoided in practical usage. The last singularity $N_2 = 0$ implies the first-layer singularity $(p, Re_3) = 0$. The detailed derivation of this equality is provided in the appendix.

In summary, there are four singular conditions represented by $\ddot{x}_{L_z} = -g$, $p_3 = 0$, $R(3,3) = 0$, or $(p, Re_3) = 0$. These singularities correspond to the situations that we want to avoid in practical usage. Hence, the existence of these singularities is admissible as a controller. In particular, we need to consider these singularities when designing the reference trajectories. Our approach is easy to check that the system is singular because the analytical solution of the closed-loop system can be derived owing to the controller structure. This feature is demonstrated in the next section.

4. Numerical Simulations

In this section, we present the numerical simulation results obtained using the proposed controller, and discuss the features of the proposed approach. The first feature is that the proposed linearization is exact and linearized subsystems are entirely decoupled. Second, based on our approach, the analytical solution of the closed-loop system can be derived. Further, owing to this analytical solution, we can check in advance whether the solution is singularity free. These features are discussed by simulating saddle-shaped trajectory tracking.

The physical parameter and controller gains are detailed in **Table 2**, where F_i is the feedback gain for the i-th linear subsystem, and the provided values are rounded off. The gains are calculated as the linear quadratic regulator with the following cost function,

$$J_i = \int_0^\infty \xi_i^T \xi_i + v_i^2 \mathrm{d}t \qquad i = 1,\ldots,4,$$

where all weights are set as 1 to discuss the validity of the proposed control structure. Note that the weights of the cost function can be tuned properly for practical usage.

Table 2. Physical parameters and controller gains.

m_B [kg]	0.2
m_L [kg]	0.1
J_B [kg m^2]	$\mathrm{diag}(2,2,4) \times 10^{-3}$
l [m]	1
F_1, F_4	$\begin{bmatrix} -1.0 & -1.7 \end{bmatrix} \in \mathbb{R}^{1\times 2}$
F_2, F_3	$\begin{bmatrix} -1.0 & -4.4 & -9.1 & -11.4 & -9.1 & -4.4 \end{bmatrix} \in \mathbb{R}^{1\times 6}$

We chose the saddle shape as the reference trajectory,

$$x_d(t) = 3\cos\left(\frac{2\pi t}{T}\right),$$
$$y_d(t) = 3\sin\left(\frac{2\pi t}{T}\right),$$
$$z_d(t) = 2\cos\left(\frac{4\pi t}{T}\right) + 2,$$
$$\psi_d(t) = 0,$$

where T is a time period.

First, we set the initial state as follows:

$$x(0) = \begin{bmatrix} 1,0,0,0,\mathbf{0_3},\mathbf{0_3},\mathbf{0_3},0,0,-1,\mathbf{0_3} \end{bmatrix}^T, \quad . \quad (18)$$

where $\mathbf{0_3} = [0,0,0]$. From the initial state, we calculate the initial value of the linearized state

$$\xi_1(0) = \begin{bmatrix} -4 & 0 \end{bmatrix}^T, \quad . \quad . \quad . \quad . \quad . \quad . \quad . \quad . \quad . \quad . \quad (19)$$
$$\xi_2(0) = \begin{bmatrix} -3 & 0 & 2.4 & 0 & -1.9 & 0 \end{bmatrix}^T, \quad . \quad (20)$$
$$\xi_3(0) = \begin{bmatrix} 0 & -2.7 & 0 & 2.2 & 0 & -1.7 \end{bmatrix}^T, \quad (21)$$
$$\xi_4(0) = \begin{bmatrix} 0 & 0 \end{bmatrix}^T, \quad . \quad . \quad . \quad . \quad . \quad . \quad . \quad . \quad . \quad . \quad (22)$$

where ξ_i is the state of the i-th linear subsystem. Next, we derived the solution of the linear differential equation corresponding to the linearized subsystems as follows,

$$\xi_i(t) = \exp\left((A_i + B_i F_i)t\right)\xi_i(0), \qquad i = 1,\ldots,4$$

where A_i, B_i are the Brunovsky canonical forms corresponding to Eqs. (8) and (15)–(17). Subsequently, the time evolution of the original state was calculated by the property of differential flatness (for details, refer to [6, 16]). To obtain a sample of the time evolution of the original state, the load position was calculated as the analytical solution, as depicted in **Fig. 2**. Note that **Fig. 2** shows the transient response calculated analytically from the initial state as well as the response on the reference trajectory.

Moreover, we can check the singularities during the time evolution in advance. **Fig. 3** depicts the transition of β_1 and $\det(\beta_2)$, respectively. Each value transitions in positive real, due to which, there is no singularity.

Next, we check the singularity when the time period of the reference trajectory is changed. As discussed in Section 3.3, one of the singularities is $\ddot{x}_{L_z} = -g$. In the case of the saddle-shaped trajectory defined in Eqs. (19)–

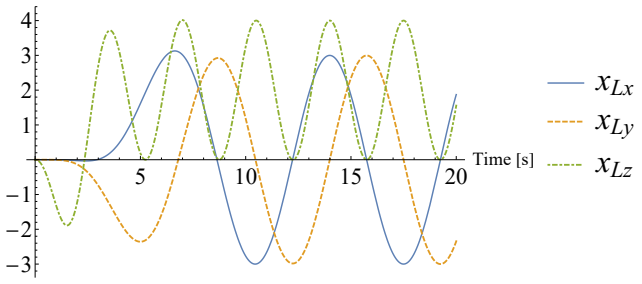

Fig. 2. The time evolution of the load position calculated using the analytical solution of the nonlinear differential equation with time period $T = 7$.

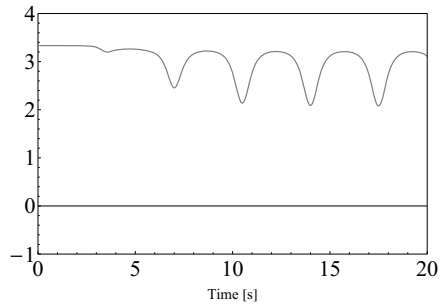

(a) The time evolution of the value of $\beta_1 := \mathscr{L}_{g_{01}} \dot{h}_1$.

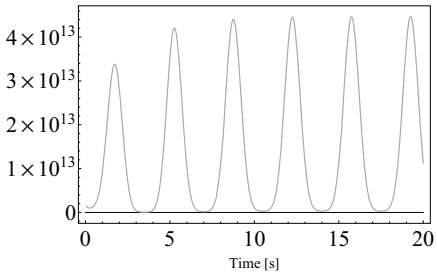

(b) The time evolution of the value of $\det(\beta_2)$.

Fig. 3. The responses of the value for singularity check with time period $T = 7$. Singularity does not exist because each value does not cross 0.

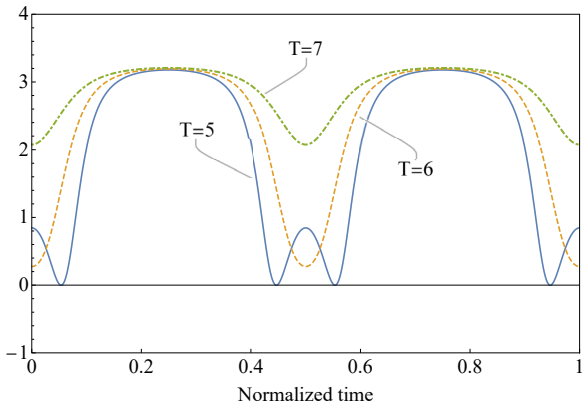

(a) The time evolution of the value of $\beta_1 := \mathscr{L}_{g_{01}} \dot{h}_1$.

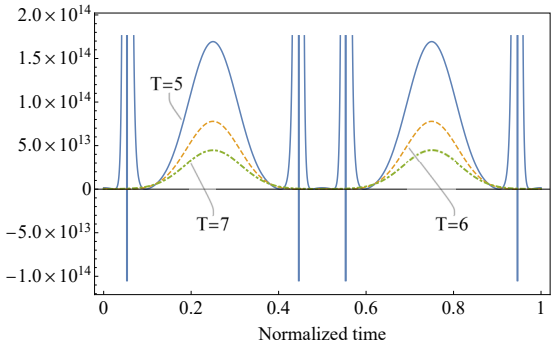

(b) The time evolution of the value of $\det(\beta_2)$.

Fig. 4. These graphs show the singularity check by the value of $\beta_1 := \mathscr{L}_{g_{01}} \dot{h}_1$ and $\det(\beta_2)$ with the time period variations. The horizontal scale is normalized by time period t/T. The trajectory in the case of $T = 5$ goes through a singular state.

(22), this singularity is satisfied at $T = \sqrt{32\pi^2/g}$. The magnitude of the vertical acceleration increases when the time period T becomes faster. Therefore, the time period T should be larger than $\sqrt{32\pi^2/g} \approx 5.67$. On the reference trajectory, the singularity condition $p_3 = 0$ is equal to $\ddot{x}_{L_z} = -g$. On the other hand, the relations between the time period and the remaining conditions $(p, Re_3) = 0$ and $R(3,3) = 0$ are too complex to be checked analytically. However, by considering the natural assumption that the cable is tensioned on the smooth reference trajectory, the load remains lower than the drone with respect to the body-fixed frame. This implies that $(p, Re_3) \neq 0$. When we design the reference trajectory such that $\ddot{x}_{L_z} > -g$, $R(3,3)$ is not zero because the thrust force points towards the upper half-space, which cancels the gravitational force. These intuitive analyses were verified numerically as follows.

To evaluate the reference trajectory, the initial state was considered on the reference trajectory. **Fig. 4** shows the values of $\mathscr{L}_{g_{01}} \dot{h}_1$ and $\det(\beta_2)$ in one cycle with a different T. The reference trajectory faster than $T = 6$ becomes singular. The 3-dimensional plot of the reference load trajectory and the position of the drone in these time periods are depicted in **Fig. 5**. Note that the drone position when it moves faster than in the case of $T = 6$ goes under the reference load position. This analysis gives us an index to choose an appropriate trajectory, but note that this analysis works on the reference trajectory. For the transient response, the analysis is more complicated because the conditions are a function of the linear controller and the initial state.

Finally, we present the numerical simulation results controlled by Eqs. (9), (10), and (14) with time period $T = 7$, as shown in **Figs. 6** and **7**. **Fig. 6** graphs a one-cycle state response after the convergence to the reference trajectory to observe the generation of a periodic motion. Note that the norm constraints $\|q\| = 1$ and $\|p\| = 1$ are satisfied, and the angular velocity of the load is $(p, \omega) = 0$. In **Fig. 7**, the flat outputs converge to zero, and hence, the load position converges to the reference trajectory. The deviation of the time response is defined as

$$h_i(t) - L_i(t) \qquad i = 1, \ldots, 4,$$

where L_i is the linear system response corresponding to

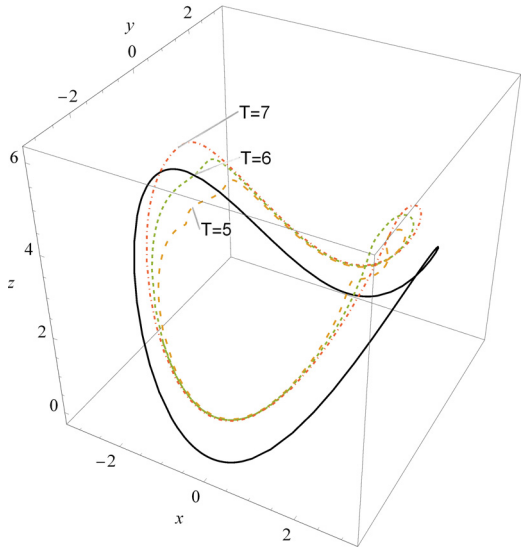

(a) Perspective view.

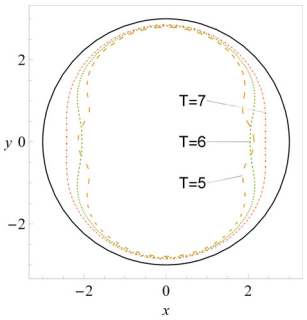

(b) Above view.

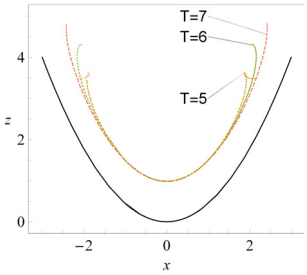

(c) Front view.

Fig. 5. Reference trajectories with a time period from 5 to 7 seconds, respectively. The solid line is the load reference trajectory, whereas the dashed lines are the drone trajectories.

the i-th linearized system with the corresponding initial state. The error remains zero in each graph, and therefore, we can conclude that the coupling among the flat outputs is adequately canceled.

5. Conclusion

In this study, we revealed that the exact linearization method, called hierarchical linearization, is applicable to a drone with a cable-suspended load. The proposed approach has a singularity in the input transformation to decouple the subsystems. A detailed analysis of the singularity was conducted, and the physical interpretation of the singular state was provided.

One of the advantages of exact linearization is that the analytical solution of the nonlinear system can be obtained. The procedure to derive the analytical solution of the closed-loop system is demonstrated in Section 4. Moreover, the singularity of the input transformation was evaluated using the proposed solution. The singularity analysis provides valuable information for designing the

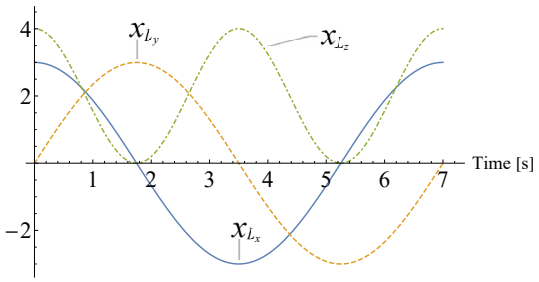

(a) Time evolution of x_L.

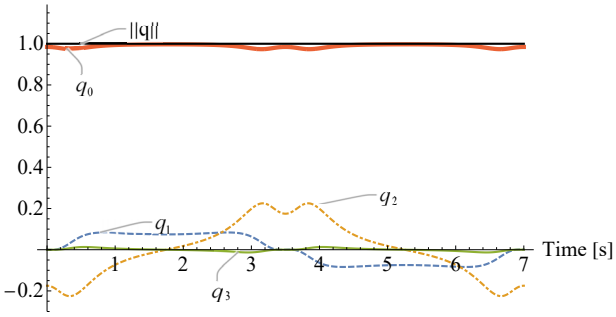

(b) Time evolution of q and its norm value.

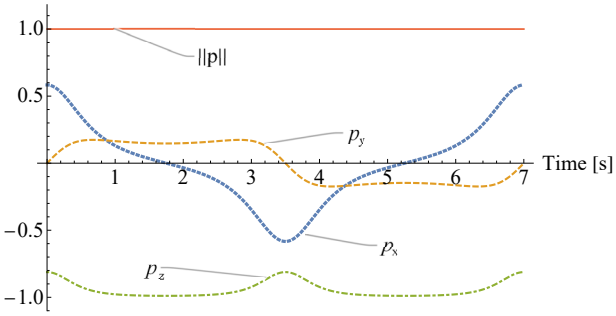

(c) Time evolution of p and its norm value.

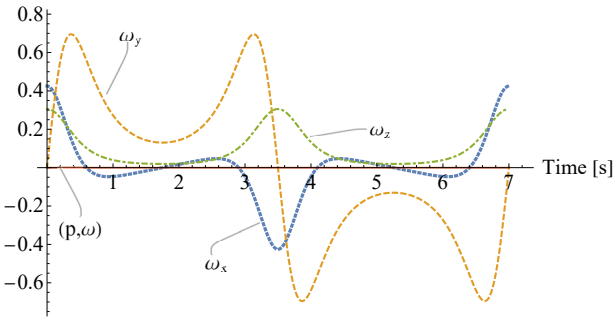

(d) Time evolution of ω and the value of (p, ω).

Fig. 6. Results of the numerical simulation. The one-period data after the trajectory converges to the reference is depicted. (b), (c), and (d) depict that the two norm constraints and the rotation angle around p maintain an approximately constant value.

reference trajectory. For the selected trajectory, a numerical simulation of the trajectory tracking control based on hierarchical linearization was conducted. Through this simulation, we proved the validity of the proposed linearization approach and that the proposed controller can achieve trajectory tracking.

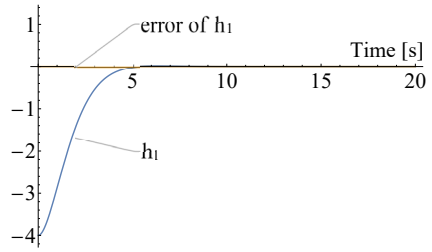

(a) Time evolution of h_1 and the deviation from the linear simulation.

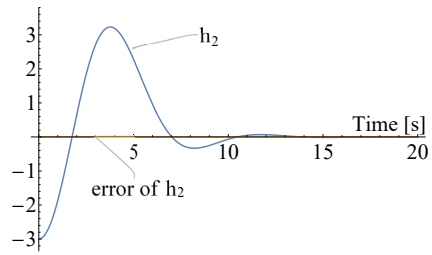

(b) Time evolution of h_2 and the deviation from the linear simulation.

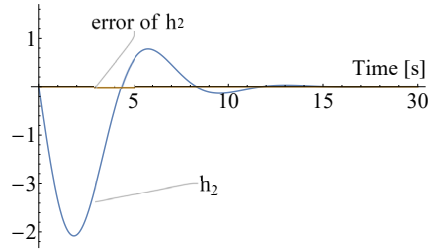

(c) Time evolution of h_3 and the deviation from the linear simulation.

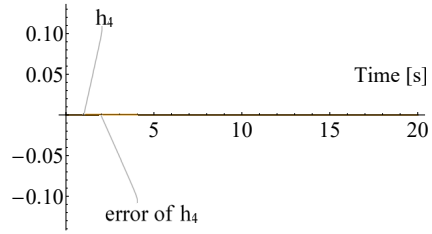

(d) Time evolution of h_4 and the deviation from the linear simulation.

Fig. 7. Results of the numerical simulation. The virtual output converges to zero, and its time response is equal to the corresponding linear response.

References:

[1] K. Nonami, "Research and development of drone and roadmap to evolution," J. Robot. Mechatron., Vol.30, No.3, pp. 322-336, 2018.

[2] X. Ding, P. Guo, K. Xu, and Y. Yu, "A review of aerial manipulation of small-scale rotorcraft unmanned robotic systems," Chinese J. of Aeronautics, Vol.32, No.1, pp. 200-214, 2019.

[3] D. K. D. Villa, A. S. Brandão, and M. Sarcinelli-Filho, "A Survey on Load Transportation Using Multirotor UAVs," J. of Intelligent and Robotic Systems: Theory and Applications, Vol.98, No.2, pp. 267-296, 2020.

[4] R. Kellermann, T. Biehle, and L. Fischer, "Drones for parcel and passenger transportation: A literature review," Transportation Research Interdisciplinary Perspectives, Vol.4, 100088, 2020.

[5] I. Palunko, P. Cruz, and R. Fierro, "Agile load transportation: Safe and efficient load manipulation with aerial robots," IEEE Robotics and Automation Magazine, Vol.19, No.3, pp. 69-79, 2012.

[6] K. Sreenath, N. Michael, and V. Kumar, "Trajectory generation and control of a quadrotor with a cable-suspended load – A differentially-flat hybrid system," 2013 IEEE Int. Conf. on Robotics and Automation, pp. 4888-4895, 2013.

[7] K. Sreenath, T. Lee, and V. Kumar, "Geometric Control and Differential Flatness of a Quadrotor UAV with a Cable-Suspended Load," 52nd IEEE Conf. on Decision and Control, pp. 2269-2274, 2013.

[8] A. Faust, I. Palunko, P. Cruz, R. Fierro, and L. Tapia, "Automated aerial suspended cargo delivery through reinforcement learning," Artificial Intelligence, Vol.247, pp. 381-398, 2017.

[9] C. Y. Son, H. Seo, T. Kim, and H. Jin Kim, "Model Predictive Control of a Multi-Rotor with a Suspended Load for Avoiding Obstacles," Proc. of IEEE Int. Conf. on Robotics and Automation, pp. 5233-5238, 2018.

[10] M. Fliess, "Generalized controller canonical form for linear and nonlinear dynamics," IEEE Trans. on Automatic Control, Vol.35, No.9, pp. 994-1001, 1990.

[11] M. Fliess, J. Lévine, P. Martin, and P. Rouchon, "Flatness and defect of non-linear systems: introductory theory and examples," Int. J. of Control, Vol.61, No.6, pp. 1327-1361, 1995.

[12] M. Fliess, C. Join, and H. Sira-Ramírez, "Non-linear estimation is easy," Int. J. of Modelling, Identification and Control, Vol.4, No.1, pp. 12-27, 2008.

[13] K. Sekiguchi, "Stabilization of three-link acrobot via hierarchical linearization," 54rd IEEE Conf. on Decision and Control, pp. 7808-7813, 2015.

[14] K. Sekiguchi, "Novel control method for quadcopter-hierarchical linearization approach," 2017 11th Asian Control Conf., pp. 1853-1858, 2017.

[15] M. Ishikawa and M. Sampei, "On equlibria set and feedback stabilizability of nonolinear control systems," IFAC Symposium on Nonlinear Control Systems, pp. 637-642, 1998.

[16] D. Mellinger and V. Kumar, "Minimum snap trajectory generation and control for quadrotors," Proc. of IEEE Int. Conf. on Robotics and Automation, pp. 2520-2525, 2011.

Appendix A. A Proof that $N_2 = 0$ Equals $(p, Re_3) = 0$

The dynamics of the center of mass of the system is

$$\begin{aligned}(m_B + m_L)\ddot{x}_c &= m_B\ddot{x}_B + m_L\ddot{x}_L \\ &= fRe_3 - (m_B + m_L)ge_3,\end{aligned}$$

where x_c is the center of mass. By substituting the relation Eq. (7) into the second equality, the z-axis term is

$$(m_B + m_L)(\ddot{x}_{Lz} + g) - m_B l\ddot{p}(3) - fR(3,3) = 0. \quad (23)$$

The dynamics of x_{Lz} is

$$m_B\ddot{x}_{Lz} = m_B\left(\ddot{h}_1 + \ddot{z}_d\right) = m_B\left(v_1 + \ddot{z}_d\right) = F_{Lz} - m_B g,$$

where F_{Lz} is a force acting on x_{Lz}. From the last equality, we get

$$\frac{F_{Lz}}{m_B} = v_1 + g + \ddot{z}_d = N_1.$$

Therefore,

$$N_2 = (m_L + m_B)(\ddot{x}_{Lz} + g) + lm_B(\omega, \omega)p(3). \quad . \quad (24)$$

Now by calculating $\ddot{p}$, we get

$$lm_B(\omega, \omega)p = -m_B l\ddot{p} + p \times (p \times fRe_3). \quad . \quad . \quad (25)$$

Finally, we transform N_2 using Eqs. (25) and (23). Then, we have

$$\begin{aligned}N_2 &= (m_L + m_B)(\ddot{x}_{Lz} + g) - m_B l\ddot{p}(3) \\ &\quad + (p \times (p \times fRe_3))(3) \\ &= f\left((p \times (p \times fRe_3))(3) + R(3,3)\right).\end{aligned}$$

The vector $p \times (p \times Re_3)$ is depicted in **Fig. 8**, and this indicates that $(p \times (p \times fRe_3))(3) + Re_3 = 0$ if and only if $(p, Re_3) = 0$. □

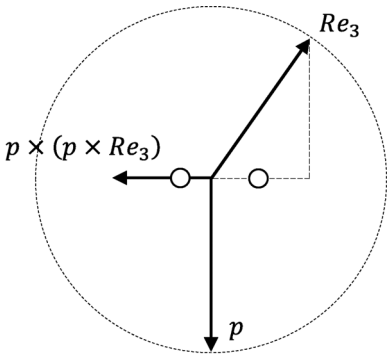

Fig. 8. Geometric relation of p, Re_3, and $p \times (p \times Re_3)$. The two small circles indicate the same length.

Name:
Kazuma Sekiguchi

Affiliation:
Department of Mechanical Systems Engineering, Faculty of Engineering, Tokyo City University

Address:
1-28-1 Tamazutsumi, Setagaya-ku, Tokyo 158-8557, Japan

Brief Biographical History:
2010 Received Doctor of Engineering from Tokyo Institute of Technology
2010- Assistant Professor, Tokyo Institute of Technology
2013- Assistant Professor, Tokyo City University
2015- Lecturer, Tokyo City University
2019- Associate Professor, Tokyo City University

Main Works:
• Nonlinear systems control, underactuated system control, UAV control

Membership in Academic Societies:
• The Institute of Electrical and Electronics Engineers (IEEE)
• The Society of Instrument and Control Engineers (SICE)
• The Institute of Systems, Control and Information Engineers (ISCIE)
• The Japan Society of Mechanical Engineers (JSME)

Name:
Wataru Eikyu

Affiliation:
Department of Mechanical Systems Engineering, Faculty of Engineering, Tokyo City University

Address:
1-28-1 Tamazutsumi, Setagaya-ku, Tokyo 158-8557, Japan

Brief Biographical History:
2017- Bachelor Student, Tokyo City University

Main Works:
• Geometric UAV control

Membership in Academic Societies:
• The Society of Instrument and Control Engineers (SICE)

Name:
Kenichiro Nonaka

Affiliation:
Department of Mechanical Systems Engineering, Faculty of Engineering, Tokyo City University

Address:
1-28-1 Tamazutsumi, Setagaya-ku, Tokyo 158-8557, Japan

Brief Biographical History:
1997 Received Doctor of Engineering from Tokyo Institute of Technology
1997- Research Assistant, Musashi Institute of Technology
2000- Lecturer, Musashi Institute of Technology
2007- Associate Professor, Musashi Institute of Technology
2013- Professor, Tokyo City University

Main Works:
• Model predictive control, moving horizon estimation, vehicle control

Membership in Academic Societies:
• The Society of Instrument and Control Engineers (SICE)
• The Institute of Electrical and Electronics Engineers (IEEE)
• The Japan Society of Mechanical Engineers (JSME)